PHYSICS

Many-body topological invariants from randomized measurements in synthetic quantum matter

Andreas Elben[1,2]*, Jinlong Yu[1,2]*, Guanyu Zhu[3†], Mohammad Hafezi[3,4], Frank Pollmann[5,6], Peter Zoller[1,2], Benoît Vermersch[1,2,7‡]

Many-body topological invariants, as quantized highly nonlocal correlators of the many-body wave function, are at the heart of the theoretical description of many-body topological quantum phases, including symmetry-protected and symmetry-enriched topological phases. Here, we propose and analyze a universal toolbox of measurement protocols to reveal many-body topological invariants of phases with global symmetries, which can be implemented in state-of-the-art experiments with synthetic quantum systems, such as Rydberg atoms, trapped ions, and superconducting circuits. The protocol is based on extracting the many-body topological invariants from statistical correlations of randomized measurements, implemented with local random unitary operations followed by site-resolved projective measurements. We illustrate the technique and its application in the context of the complete classification of bosonic symmetry-protected topological phases in one dimension, considering in particular the extended Su-Schrieffer-Heeger spin model, as realized with Rydberg tweezer arrays.

INTRODUCTION

There is an increasing interest in realizing topological quantum phases in synthetic quantum systems (*1*–*5*), including ultracold atoms in optical lattices (*2*), Rydberg atoms (*3*), trapped ions (*4*), and superconducting qubits (*5*). These experimental platforms offer unique possibilities for preparing, controlling, and probing quantum states, with prospects of studying these exotic states of matter, e.g., the fractional Hall state (*6*, *7*), and in light of possible applications such as topological quantum computing (*8*). The characterization and identification of topological phases in an experimental setting represents, however, a substantial challenge: In contrast to symmetry-breaking phases of Landau's theory with local order parameters (*9*), topological phases are characterized by global properties, which cannot be revealed with local probes. Thus, measurement protocols need to be developed to access these global properties. For noninteracting systems, the measurement of topological invariants (such as the Chern number) has been achieved in seminal experiments in cold atom setups (*10*–*13*), microwave networks (*14*), and photonic systems (*15*). Below, we address the generic interacting case, and we present measurement protocols that allow us to access many-body topological invariants (MBTIs) of interacting topological states with global symmetries (*16*, *17*).

MBTIs are highly nonlocal quantized correlators of the many-body wave function that have been originally derived in the context of the description of symmetry-protected topological (SPT) order (*18*), and in particular from the classification of unidimensional bosonic SPT phases (*16*, *17*, *19*). An MBTI identifies from a many-body wave function the projective representation of a global symmetry (*16*, *17*). For any realization of a topological state with a given symmetry, for instance, the spatial reflection symmetry or the time-reversal symmetry, the corresponding MBTI takes a non-zero quantized value. MBTIs can be considered as generalizations of string order parameters that were introduced (*20*) and measured (*21*, *22*) to detect SPT phases protected by internal symmetries. MBTIs can particularly identify all one-dimensional bosonic SPT phases, even in the absence of internal symmetries, and therefore of string order (*17*, *23*). MBTIs are not restricted to the description of SPT phases: They have been now understood in the general mathematical framework of topological quantum field theory (*17*, *24*, *25*), suggesting that they can identify many types of topological phases beyond SPT orders. In particular, recent theoretical works have shown that MBTIs can identify fermionic SPT phases (*24*, *26*) and topological quantum phase transitions (*27*) and can also distinguish various symmetry-enriched topological (SET) phases with intrinsic topological orders (*28*, *29*). Whereas MBTIs have become key quantities to characterize topology in synthetic quantum systems, the question of their measurement has remained so far elusive.

Our approach to measure MBTIs consists in using the information contained in statistical correlations between randomized measurements. These measurements are realized by applying to a quantum state a sequence of random unitary operations before performing projective measurements. Recently, randomized measurement protocols have been developed to measure entanglement (*30*, *31*), including an experimental demonstration in a trapped-ion quantum simulator (*32*), and out-of-time order correlators (*33*). Here, our approach is based on local random unitaries that can be implemented in experiments with high fidelities (*32*), and the key idea is to use distributions of such random unitaries with different symmetries. From the statistics of such "symmetric" randomized measurements, one can extract the MBTI associated with a particular symmetry. Our analysis of the protocol, including the study of statistical errors, shows that MBTIs can be measured via our protocols with current technology in various spin systems, such as Rydberg atoms, trapped ions, and superconducting qubits, and can be used to experimentally classify interacting many-body topological quantum phases.

Our article is organized as follows. Having in mind current experimental possibilities, e.g., with Rydberg atom quantum simulators (*22*), we study a model Hamiltonian with SPT phases as ground

[1]Center for Quantum Physics, University of Innsbruck, Innsbruck A-6020, Austria. [2]Institute for Quantum Optics and Quantum Information of the Austrian Academy of Sciences, Innsbruck A-6020, Austria. [3]Joint Quantum Institute, NIST/University of Maryland, College Park, MD 20740, USA. [4]Institute for Research in Electronics and Applied Physics, University of Maryland, College Park, MD 20742, USA. [5]Department of Physics, Technical University of Munich, 85748 Garching, Germany. [6]Munich Center for Quantum Science and Technology, Schellingstr. 4, D-80799 München, Germany. [7]Univ. Grenoble Alpes, CNRS, LPMMC, 38000 Grenoble, France.
*These authors contributed equally to this work.
†Present address: IBM T.J. Watson Research Center, Yorktown Heights, NY 10598, USA.
‡Corresponding author. Email: benoit.vermersch@lpmmc.cnrs.fr

states. We consider MBTIs associated with reflection and time-reversal symmetries to identify the trivial/nontrivial topology of the SPT phases as well as the symmetry-broken phase, and present the corresponding measurement protocols as experimental recipes; the other MBTIs and corresponding protocols are presented in the Supplementary Materials. We then discuss the role of statistical errors and imperfections in our scheme. We also illustrate our protocols via two physical examples that can be realized in experiments: We show how to monitor the dynamical building-up of topology by these MBTIs during adiabatic state preparation, and we also discuss how the breaking and protection mechanisms of symmetries can be probed experimentally. Last, we discuss how our protocols can be applied beyond the case of SPT phases.

RESULTS

Model

For concreteness, we present our approach in the context of the extended bosonic Su-Schrieffer-Heeger (SSH) model (Fig. 1A) (*22*, *34*–*37*)

$$H_{\mathrm{eSSH}} = \frac{J}{2}\sum_{i=1}^{N/2}\left(\sigma_{2i-1}^{x}\sigma_{2i}^{x} + \sigma_{2i-1}^{y}\sigma_{2i}^{y} + \delta\sigma_{2i-1}^{z}\sigma_{2i}^{z}\right) + \frac{J'}{2}\sum_{i=1}^{N/2-1}\left(\sigma_{2i}^{x}\sigma_{2i+1}^{x} + \sigma_{2i}^{y}\sigma_{2i+1}^{y} + \delta\sigma_{2i}^{z}\sigma_{2i+1}^{z}\right) \quad (1)$$

Here, σ_i^{μ} ($\mu = x, y, z$) are the Pauli matrices for the spin state at site *i*. J and J' are alternating nearest-neighbor spin-exchange coefficients, and δ denotes the exchange anisotropy. The case of $\delta = 1$ corresponds to the bond-alternating Heisenberg model (*35*, *36*), whereas the case of $\delta = 0$ corresponds to the bosonic version of the (non-interacting) SSH model (*34*), as realized recently with Rydberg atoms (*22*). Note that, expect for $\delta = 0$ and $\delta = 1$, the model is generally not integrable and thus has no single-particle correspondence. The alternating spin-exchange coefficients can be engineered, e.g., by loading bosonic atoms into optical superlattices (*37*) or dimerized optical tweezer arrays (*22*), or by coupling bosonic atoms to dynamical gauge fields (*38*, *39*). As a final remark, we emphasize that all protocols presented below can also be generalized to other spin Hamiltonians, e.g., spin-1 Haldane chain (*40*), straightforwardly.

As shown below, the model Hamiltonian in Eq. 1 hosts three different phases: a trivial phase, a topological Haldane phase (*40*), and a symmetry-broken antiferromagnetic phase. The trivial and topological phases are SPT phases protected by any one of the following three symmetries (*23*, *41*): reflection (inversion) symmetry at the center bond, time-reversal symmetry, and dihedral group D_2 of π-rotations of spins around the *x*, *y*, and *z* axes.

Partial reflection invariant

We now show how to measure MBTIs via randomized measurements. First, SPT phases protected by reflection symmetry can be classified using the partial reflection MBTI $\widetilde{\mathcal{Z}}_{\mathcal{R}} = \mathcal{Z}_{\mathcal{R}}/\sqrt{\left[\mathrm{Tr}\left(\rho_{I_1}^2\right) + \mathrm{Tr}\left(\rho_{I_2}^2\right)\right]/2}$ (*17*), with

$$\mathcal{Z}_{\mathcal{R}} = \mathrm{Tr}(\rho_I \mathcal{R}_I) \quad (2)$$

Here, $\rho_I = \mathrm{Tr}_{S-I}(|\psi\rangle\langle\psi|)$ is the reduced density matrix of a many-body quantum state $|\psi\rangle$, and the interval $I = I_1 \cup I_2$ consists of two partitions I_1 and I_2, each with *n* sites; *S* denotes all the sites of the system. The nonlocal operator $\mathcal{R}_I$ "spatially swaps" I_1 and I_2 with respect to the reflection center. On every basis state $|s_I\rangle = |s_1, s_2, \ldots, s_{2n}\rangle$ ($s_i = \uparrow, \downarrow$ for $i \in I$), it acts as $\mathcal{R}_I|s_I\rangle = |s_{2n}, s_{2n-1}, \ldots, s_1\rangle \equiv |\mathcal{R}_I(s_I)\rangle$. This operation is graphically shown in Fig. 1B, where the state of each site of *I*, represented as a blue line, is "contracted" with the state of the mirror symmetric site.

The MBTI $\widetilde{\mathcal{Z}}_{\mathcal{R}}$ probes the action of the reflection symmetry on the many-body state $|\psi\rangle$. Using tensor-network theory, one can show analytically that, for the ground state of a gapped many-body Hamiltonian (e.g., H_{eSSH}), $\widetilde{\mathcal{Z}}_{\mathcal{R}}$ approaches a quantized value in the thermodynamic limit $n, N \to \infty$ (*17*). The typical value of *n* required to achieve convergence is determined by the correlation length in the system and is discussed in detail below. For our model Eq. 1, the phase diagram evaluated by the MBTI $\widetilde{\mathcal{Z}}_{\mathcal{R}}$, calculated numerically using the density matrix renormalization group (DMRG) method (see Materials and Methods for details), is shown in Fig. 1C. Three phases can be identified therein: (i) a phase with antiferromagnetic order where reflection symmetry is spontaneously broken with $\widetilde{\mathcal{Z}}_{\mathcal{R}} = 0$, (ii) the trivial SPT phase with $\widetilde{\mathcal{Z}}_{\mathcal{R}} = +1$, and (iii) the nontrivial SPT phase with $\widetilde{\mathcal{Z}}_{\mathcal{R}} = -1$.

The MBTI $\widetilde{\mathcal{Z}}_{\mathcal{R}}$, which is a highly nonlocal and nonlinear functional of the reduced density matrix ρ_I, can be measured with randomized measurements, with the following recipe (as illustrated in Fig. 1D): (i) One first prepares the ground state $|\psi\rangle$ via, e.g., adiabatic state preparation (see a later section for details). (ii.a) One applies to $|\psi\rangle$ a unitary operation $U_{\mathcal{R}}$ of the form $U_{\mathcal{R}} = \bigotimes_{i=1}^{2n} U_i$, with $U_i = U_{2n-i+1}$. The unitaries U_i ($i = 1,2, \ldots, n$) are drawn randomly from the circular unitary ensemble (CUE) defined on the local Hilbert spaces of individual spins. This type of random unitaries with spatial reflection symmetry (i.e., with a configuration $U_1U_2\ldots U_n\,|\,U_n\ldots U_2U_1$ as shown schematically in Fig. 1D) will be essential to be able to extract $\widetilde{\mathcal{Z}}_{\mathcal{R}}$ from randomized measurements. Each local unitary U_i can be decomposed in products of spin rotations along two axes (*x*,*z*) and can thus be generated with high fidelity in quantum simulators with single-site control, as also shown in recent experiments (*32*). Note that the impact of potential imperfections, such as miscalibration and decoherence, has been studied in detail in (*42*), showing the robustness and the applicability of protocols relying on randomized measurements in state-of-the-art quantum devices based on Rydberg atoms, trapped ions, or superconducting qubits. (ii.b) One measures the occupation probabilities $P_{U_{\mathcal{R}}}(s_I) = \langle s_I|U_{\mathcal{R}}\rho_I U_{\mathcal{R}}^{\dagger}|s_I\rangle$ of the basis states s_I, by performing projective measurements in the basis s_I. (iii) One repeats (i) to (ii) for many independently sampled random unitaries $U_{\mathcal{R}}$.

Given the set of outcome probabilities $P_{U_{\mathcal{R}}}(s_I)$, one obtains first $\mathcal{Z}_{\mathcal{R}}$ from

$$\mathcal{Z}_{\mathcal{R}} = 2^n \sum_{s_I} (-2)^{-\frac{1}{2}D[s_I, \mathcal{R}_I(s_I)]}\,\overline{P_{U_{\mathcal{R}}}(s_I)} \quad (3)$$

Here, $\overline{\cdots}$ denotes the ensemble average over the random unitaries and $D[s_I, \mathcal{R}(s_I)] \equiv \#\{i \in I | s_i \neq s_{2n-i+1}\}$ is the Hamming distance between $|s_I\rangle$ and $|\mathcal{R}_I(s_I)\rangle$. Equation 3 can be proven using the two-design identities of the CUE (see Materials and Methods) and shows that the MBTI $\mathcal{Z}_{\mathcal{R}}$ can be directly extracted from the statistics of randomized measurements. Second, the purity $\mathrm{Tr}\left(\rho_{I_1}^2\right)$ (and similarly $\mathrm{Tr}\left[\rho_{I_2}^2\right]$) is estimated using the relation (*31*, *32*)

$$\mathrm{Tr}\left(\rho_{I_1}^2\right) = 2^n \sum_{s_{I_1}, s'_{I_1}} (-2)^{-D[s_{I_1}, s'_{I_1}]}\,\overline{P_{U_{\mathcal{R}}}(s_{I_1})P_{U_{\mathcal{R}}}(s'_{I_1})} \quad (4)$$

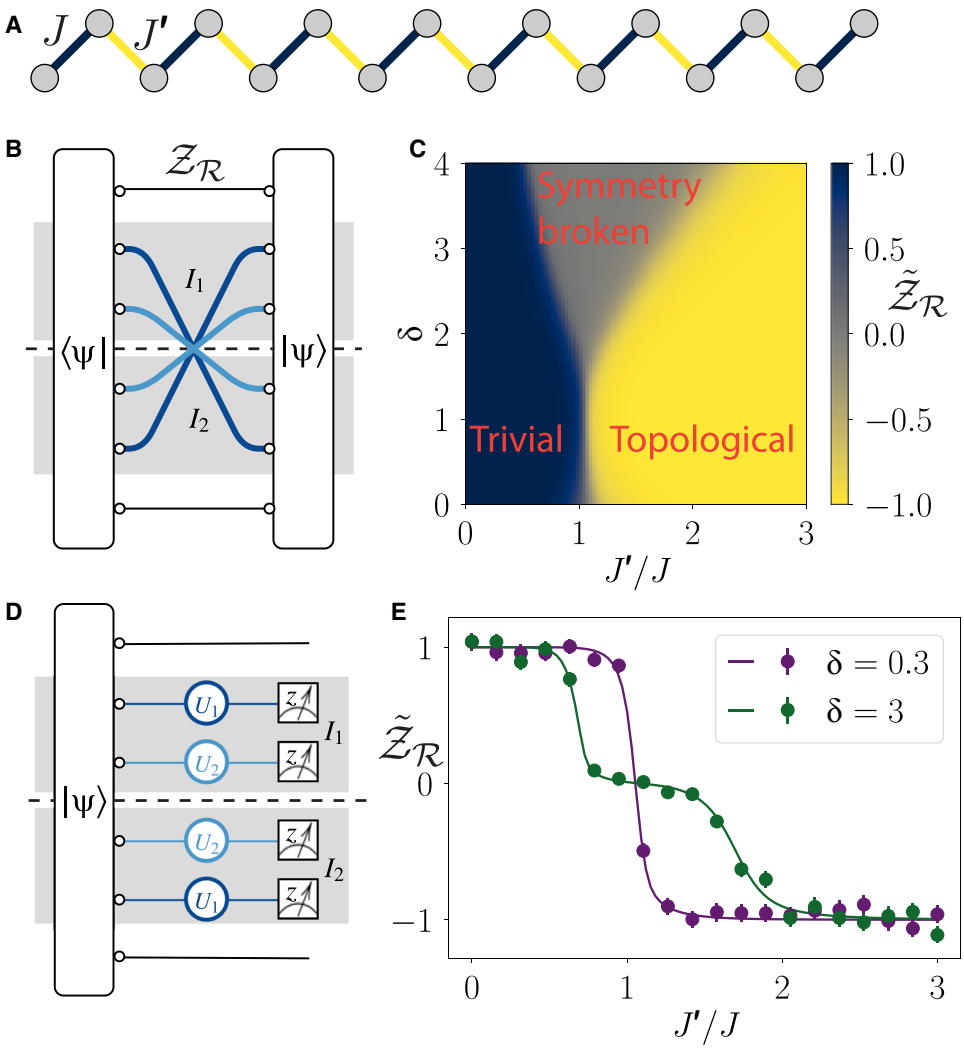

Fig. 1. Measuring the MBTI $\mathcal{Z}_\mathcal{R}$ for the extended bosonic SSH model. (**A**) Schematic illustration of the model Eq. 1, where the nearest-neighbor spin-exchange coefficients alternate between the bonds. (**B**) The partial reflection invariant $\mathcal{Z}_\mathcal{R}$ (Eq. 2) is defined as the expectation value of a partial reflection operator $\mathcal{R}_I$ (visualized by the blue lines) for the many-body state $|\psi\rangle$. The dashed line between the intervals I_1 and I_2 indicates the reflection center. (**C**) In terms of the normalized invariant $\tilde{\mathcal{Z}}_\mathcal{R}$, the full-phase diagram of the extended bosonic SSH model is revealed here for a system size of $N = 48$ spins and $n = 6$ reflected pairs of spins. We find three phases with different quantized values of $\tilde{\mathcal{Z}}_\mathcal{R}$. (**D**) Protocol to measure $\tilde{\mathcal{Z}}_\mathcal{R}$ via statistical correlations between randomized measurements, implemented with local random unitaries applied symmetrically around the central bond. (**E**) The results of simulated experiments allow us to identify topological phase transitions. The solid lines are results from DMRG, whereas the dots with error bars represent estimations from simulated randomized measurements with $N_\mathrm{U} = 512$ unitaries and $N_\mathrm{M} = 256$ measurements per unitary.

with the reduced probabilities $P_{U_\mathcal{R}}(s_I) = \mathrm{Tr}\left(|s_{I_1}\rangle\langle s_{I_1}|U_\mathcal{R}\,\rho_I\,U_\mathcal{R}^\dagger\right)$. Thus, we obtain the normalized MBTI from the second-order correlations of randomized measurements, implemented with local random operations with a distribution that is tailored to identify a certain symmetry (here, the reflection symmetry) of the many-body quantum state. This is the key idea in our approach, and we show below how to apply it to measure any MBTI. For illustration, we show in Fig. 1E the value of $\tilde{\mathcal{Z}}_\mathcal{R}$ (i) calculated from the DMRG method (line) and (ii) estimated from simulated randomized measurements (dots). They coincide with each other within the statistical errors that originate from the finite number of unitaries N_U and the finite number of projective measurements per unitary N_M. A detailed discussion about the statistical errors and imperfections for the MBTIs ($\tilde{\mathcal{Z}}_\mathcal{R}$ here and $\tilde{\mathcal{Z}}_\mathcal{T}$ below) estimated from randomized measurements can be found in a later section and the Supplementary Materials.

Partial time-reversal invariant

We now present the protocol to measure the MBTI associated with the time-reversal symmetry $\tilde{\mathcal{Z}}_\mathcal{T} = \mathcal{Z}_\mathcal{T}/\left(\left[\mathrm{Tr}\left(\rho_{I_1}^2\right)+\mathrm{Tr}\left(\rho_{I_2}^2\right)\right]/2\right)^{3/2}$ (*17*, *25*), with

$$\mathrm{Z_T} = \mathrm{Tr}\left(\rho_I u_\mathrm{T} \rho_I^{T_1} u_\mathrm{T}^\dagger\right) \tag{5}$$

Here, T_1 denotes the partial transpose operation on the partition I_1, and $u_\mathcal{T} = \prod_{i\in I_1}\sigma_i^y$ is the unitary part of the time-reversal operator. The contraction operation resulting in $\mathcal{Z}_\mathcal{T}$ is illustrated graphically in Fig. 2A.

The MBTI $\tilde{\mathcal{Z}}_\mathcal{T}$ is a nonlinear functional of two copies of the (partially transposed) density matrix ρ_I, which can be measured via the following recipe (Fig. 2B). After (i) the state preparation, we perform two experiments: (ii.a.1) In the first experiment, we apply

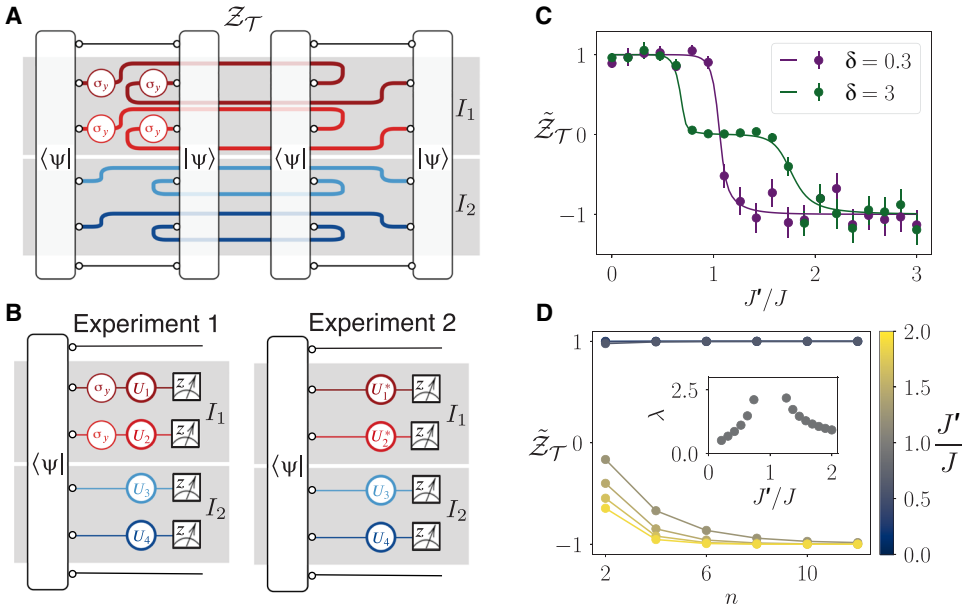

Fig. 2. Probing the MBTI $\mathcal{Z}_\mathcal{T}$ with randomized measurements. (**A**) Graphical representation of the definition of the time-reversal invariant $\mathcal{Z}_\mathcal{T}$ (Eq. 5) involving partial transpose (red lines) and partial swap (blue lines) operations. (**B**) Experimental protocol to measure $\mathcal{Z}_\mathcal{T}$ with two experiments, which are correlated using randomized measurements. To account for the anti-unitarity of the time-reversal symmetry, the local random unitaries applied in I_1 (red) in the two experiments are complex conjugate to each other. (**C**) Simulated measurements of $\tilde{\mathcal{Z}}_\mathcal{T}$ (dots with statistical error bars, with $N_U = 768$, $N_M = 512$), revealing the topological phase transitions in the extended bosonic SSH model as a function of $J' = J$ for two values of δ. Solid lines are calculated with the DMRG method, in a system with $N = 48$ sites, and $n = 6$ per interval I_1 and I_2. (**D**) $\tilde{\mathcal{Z}}_\mathcal{T}$ converges as a function of the partition size n to the quantized values ±1 for the case of $\delta = 0.25$. Different colors represent different values of $J' = J$. Inset: The divergence of the corresponding correlation length λ, extracted from an exponential fit on the first three values of n, can be used to detect the quantum critical point between the topological trivial (with $\tilde{\mathcal{Z}}_\mathcal{T} = 1$) and nontrivial (with $\tilde{\mathcal{Z}}_\mathcal{T} = -1$) phases.

$U_\mathcal{T}^{(1)} = U_{I_1} u_\mathcal{T} \otimes U_{I_2}$, with $U_{I_1} = \otimes_{i=1}^{n} U_i$ and $U_{I_2} = \otimes_{i=n+1}^{2n} U_i$, each U_i being taken independently from the CUE. (ii.b.1) We measure the probabilities $P_{U_\mathcal{T}^{(1)}}(s_I)$ (see the left panel of Fig. 2B). (ii.a.2) In a second experiment, we use the unitaries $U_\mathcal{T}^{(2)} = U_{I_1}^* \otimes U_{I_2}$. (ii.b.2) We measure $P_{U_\mathcal{T}^{(2)}}(s_I)$ (see the right panel of Fig. 2B). (iii) We repeat the two experiments (i and ii) with different unitaries U_i and estimate

$$\mathcal{Z}_\mathcal{T} = 2^{2n} \sum_{s_I, s'_I} (-2)^{-D[s_I, s'_I]} \overline{P_{U_\mathcal{T}^{(1)}}(s_I) P_{U_\mathcal{T}^{(2)}}(s'_I)} \qquad (6)$$

from cross-correlations of the two experiments. In addition, the purity to normalize $\mathcal{Z}_\mathcal{T}$ to $\tilde{\mathcal{Z}}_\mathcal{T}$ is obtained from the same experimental data using the relation Eq. 4.

Equation 6, which is also proven in Materials and Methods, shows that the partial time-reversal MBTI can be accessed from correlations between measurements using random unitary operations, which are complex conjugated. In Fig. 2C, we compare values of $\tilde{\mathcal{Z}}_\mathcal{T}$ obtained with the DMRG method with the ones estimated from finite number of randomized measurements. We see similar behavior of $\tilde{\mathcal{Z}}_\mathcal{T}$ in Fig. 2C compared with the one of $\tilde{\mathcal{Z}}_\mathcal{R}$ as in Fig. 1E but with larger error bars and deviation. This is because of the fact that the statistical errors scale differently as functions of N_U, N_M, and n (see the Supplementary Materials). The deviation and error bars can be reduced by increasing both N_U and N_M. Moreover, the solid lines in Figs. 1E and 2C are similar for the current case, because both the reflection and time-reversal symmetries are present in the Hamiltonian. The MBTIs can behave completely different for the case that one of the protecting symmetries is broken but the many-body ground state is still topological (see below and the section on 'Probing the breaking and the protection of symmetries').

In Fig. 2D, we also show that by extracting $\tilde{\mathcal{Z}}_\mathcal{T}$ (or similarly, $\tilde{\mathcal{Z}}_\mathcal{R}$, which is not shown here for conciseness) for different n, one can measure the correlation length λ of SPT phases, i.e., the characteristic length above which MBTIs become quantized. In particular, one can identify quantum critical points separating different SPT phases from the divergence of λ.

The two examples given above illustrate how to access MBTIs from the statistics of measurements performed after correlated local random unitary operations. In the Supplementary Materials, we show how to access MBTIs for internal symmetries and combination of symmetries. We also show how to identify the breaking/protection of different symmetries in a later section. Combined together, they provide a complete set of protocols to experimentally probe the classification of one-dimensional bosonic SPT phases.

Statistical errors and imperfections

Having described our main results relating randomized measurements to the MBTIs $\tilde{\mathcal{Z}}_\mathcal{R}$ and $\tilde{\mathcal{Z}}_\mathcal{T}$, we now comment on various potential sources of errors in implementing our protocol. First, statistical errors are due to the finite number of repetitions of the experiment used to estimate the statistical correlations between randomized measurements. As detailed in the Supplementary Materials, we find that the typical required number of measurements to access MBTIs within a given accuracy (scaling as $2^{1.5n}$ to access $\mathcal{Z}_\mathcal{R}$ for instance) are very similar to the requirements to measure state purities (*31*, *32*) and thus compatible with state-of-the-art experimental platforms of Rydberg atoms, trapped ions, and superconducting qubits with high repetition rates. Randomized measurements also feature a natural robustness with respect to decoherence,

readout errors, and errors in the implementations of random unitaries (*33*, *42*), because they are based on extracting relevant quantities from ensemble averages (and not from individual measurements). We thus expect our protocols to allow faithful measurements of MBTIs in various experimental platforms. In the following, we illustrate our protocols by means of two important applications: the dynamical building-up of nontrivial topology during the adiabatic preparation of an SPT phase and the identification of the protecting symmetry group.

Monitoring the dynamical building-up of topology

The MBTIs $\widetilde{\mathcal{Z}}_{\mathcal{R}}$ and $\widetilde{\mathcal{Z}}_{\mathcal{T}}$ can be defined for an arbitrary many-body quantum state $|\psi\rangle$ besides the ground state as described above. Thus, we can also use the presented measurement protocols to monitor the preparation of an SPT state $|\psi(t)\rangle$ as a function of time, which facilitates the visualization of the dynamical building-up of topology experimentally. For concreteness, we consider the adiabatic state preparation with a time-dependent Hamiltonian

$$H(t) = H_{\mathrm{eSSH}} + f(t)H_{\mathrm{Néel}} \tag{7}$$

where $H_{\mathrm{Néel}} = \Delta\sum_i(-1)^i\sigma_i^z$ is a staggered magnetic field term with a strength $\Delta \gg J', J$. We always set the function $f(t)$ to satisfy $f(t=0) = 1$ and $f(t=t_F) = 0$. At time $t = 0$, the system is initialized in the Néel state $|\psi(t=0)\rangle = |\downarrow\uparrow\downarrow\ \ldots\rangle$. As an example, we adopt the function $f(t) = (t/t_F - 1)^4$ to adiabatically drive the system to the ground state of H_{eSSH} at the final time $t = t_F$. Our protocols give access to the time-dependent values of MBTI $\widetilde{\mathcal{Z}}_{\mathcal{T}}(t), \widetilde{\mathcal{Z}}_{\mathcal{R}}(t)$, obtained using the experimental recipe described above with random unitaries applied on the time-dependent many-body quantum state $|\psi(t)\rangle$. We illustrate the emergence of quantized values of the MBTI $\widetilde{\mathcal{Z}}_{\mathcal{R}}(t)$ [the results for $\widetilde{\mathcal{Z}}_{\mathcal{T}}(t)$ are similar and are not shown for conciseness], associated with the preparation of the SPT phases, in Fig. 3A. Note that the preparation time $Jt_F = 20$ is compatible with the coherence time achieved in the Rydberg experiment realizing the Haldane phase of the bosonic SSH model (*22*). As shown in Fig. 3B, the values of $\widetilde{\mathcal{Z}}_{\mathcal{R}}(t_F)$ at the end of the preparation $t = t_F$ can be used to detect the quality of the preparation of an SPT phase: For $Jt_F \gg 1$, the preparation is perfectly adiabatic, and the values of the MBTI correspond to the ones of the ground state wave function (as presented in Figs. 1 and 2). For $Jt_F \sim 1$, the correlations in the wave function do not extend over the full system, as in the true SPT ground state, but only extend to certain characteristic length scale n_c. Consequently, for $n \gg n_c$, the many-body invariant tends to zero. We expect a similar behavior for a scenario where $|\psi(t=t_F)\rangle$ is replaced by a thermal state, and n_c by a "thermal length" describing the range of correlations. Our protocols can also be used to probe topology in non-equilibrium systems (*43*).

Probing the breaking and the protection of symmetries

The MBTIs $\widetilde{\mathcal{Z}}_{\mathcal{R}}$ and $\widetilde{\mathcal{Z}}_{\mathcal{T}}$ behave similarly (cf. Figs. 1E and 2C) for the model Hamiltonian H_{eSSH} in Eq. 1, because both reflection and time-reversal symmetries are respected. In addition to identifying the topology, measuring MBTIs also provides us with the ability to experimentally study the protection mechanism of SPT phases. In particular, SPT order can still exist in the absence of certain internal symmetries (thus, string order being absent), provided at least one protecting symmetry is present (*41*). To illustrate this effect with MBTIs, we add here the term

$$H_B = B\sum_{j=1}^{N-1}\left(\sigma_j^x\sigma_{j+1}^z - \sigma_j^z\sigma_{j+1}^x\right) \tag{8}$$

to the original Hamiltonian H_{eSSH}. In the Hamiltonian $H = H_{\mathrm{eSSH}} + H_B$, the reflection and D_2 symmetries are explicitly broken, but the time-reversal symmetry is respected (*43*). Thus, the ground state of $H = H_{\mathrm{eSSH}} + H_B$ can still exhibit nontrivial SPT order, protected solely by the time-reversal symmetry. This is encoded in the values of the MBTIs and can thus be revealed experimentally via our protocols. As shown in Fig. 4, the partial time-reversal MBTI $\widetilde{\mathcal{Z}}_{\mathcal{T}}$ converges to ±1 for $n \to \infty$, whereas the partial reflection MBTI $\widetilde{\mathcal{Z}}_{\mathcal{R}}$ approaches 0 as $n \to \infty$.

DISCUSSION

To conclude, the use of randomized measurements to probe topological properties of the wave function is a new paradigm that enables the experimental classification of many-body topological quantum phases. While we have focused our study on unidimensional SPT phases, our protocols also open the possibilities for probing two-dimensional SPT phases (*44*), as well as identifying different

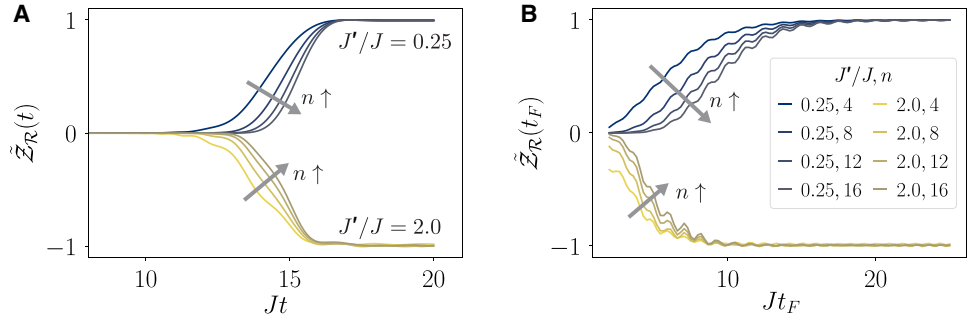

Fig. 3. Monitoring the adiabatic preparation of an SPT state. (**A**) Starting from a trivial Néel state without reflection symmetry $\widetilde{\mathcal{Z}}_{\mathcal{R}}(t)$, the ground state of H_{eSSH} is adiabatically prepared. This is monitored by the evolution of $\widetilde{\mathcal{Z}}_{\mathcal{R}}(t)$, which evolves to quantized values ±1 at late times. The dynamical buildup of long-range SPT order—for intermediate times up to a certain length scale—is indicated at intermediate times by the increasing magnitude of $\widetilde{\mathcal{Z}}_{\mathcal{R}}(t)$ for decreasing number n of reflected pairs of spins. Here, we set $Jt_F = 20$. (**B**) The convergence of $\widetilde{\mathcal{Z}}_{\mathcal{R}}(t_F)$ to ±1 as a function of the total preparation time t_F indicates that, for sufficiently long preparation times, the ground states in trivial and topological states are prepared with high fidelity. For the simulations, we use the time-evolving block decimation (TEBD) algorithm (as detailed in Materials and Methods) and set the parameters as $\delta = 0.25$, $\Delta = 40J$, and $N = 48$.

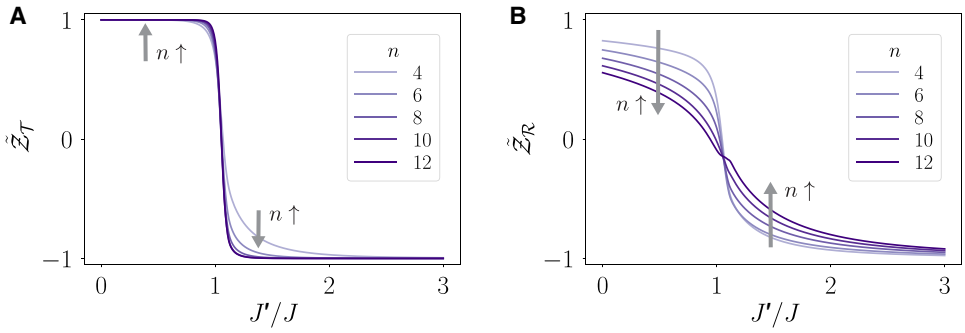

Fig. 4. Detecting the protecting symmetries for the SPT states. In the presence of the symmetry-breaking perturbation H_B (Eq. 8), the topological phase in the modified Hamiltonian $H = H_{eSSH} + H_B$ is (only) protected by the time-reversal symmetry. (**A**) This is detected by the partial time-reversal MBTI $\widetilde{\mathcal{Z}}_{\mathcal{T}}$—converging to the quantized values ±1 for increasing n—which still identifies the topological phase transition. (**B**) On the contrary, the partial reflection MBTI $\widetilde{\mathcal{Z}}_{\mathcal{R}}$—approaching 0 with increasing n—shows that the reflection symmetry is explicitly broken for a nonzero B in Eq. 8. We choose $B = 0.1J$, $\delta = 0.3$, and $N = 48$.

SET phases (*28*, *29*, *45*, *46*). The accompanied symmetries, e.g., reflection and time-reversal symmetries, for SET phases (*29*) can be distinguished via the same MBTIs as for SPT phases (defined in compactified one-dimensional geometries) and thus can also be probed via randomized measurements. We also note that our protocol—presented in this work for spin systems—can also be realized in fermionic systems (*24*) via global random unitaries implemented for example with random quenches in Hubbard systems (*31*).

As a future direction, our work also suggests that anyonic statistics describing the essence of topologically ordered states can be accessed via randomized measurements, extending, in particular, approaches based on impurities (*47*) or linear response (*48*) to measure the many-body Chern number of fractional quantum Hall states. Moreover, modular matrices revealing anyonic statistics (*49*) can be expressed as spatial reflection operators in a form analog to $\widetilde{\mathcal{Z}}_{\mathcal{R}}$ on torus geometries (*50*) and could thus be measured via randomized measurements.

MATERIALS AND METHODS

In this part, we present the proofs of Eqs. 3 to 6, relating MBTIs to statistical correlations of randomized measurements, together with the details on our DMRG and TEBD (time-evolving block decimation) simulations. Here, we also focus on the case of spin-1/2 systems. Our formulas can, however, be extended straightforwardly to the cases with higher internal dimensions (spins 1, 3/2, etc.).

Random unitary calculus

We begin by summarizing elementary properties of random unitaries from the CUE. We discuss the minimal case of two spins, each with Hilbert space $\mathcal{H}$. These can be either (i) two spins located at different lattice sites in a single many-body system (partial inversion invariant) or (ii) two spins located at the same site but realized in two different, sequentially performed, experiments (time-reversal invariant). Given a two-spin operator O acting on both spins with total Hilbert space $H^{\otimes 2}$, we define the unitary twirling channel

$$\Phi(O) \equiv \overline{U^\dagger \otimes U^\dagger O U \otimes U} \tag{9}$$

where $\overline{\cdots}$ denotes the average over random unitaries U taken from the CUE (i.e., the average with respect to the Haar measure on the group of unitary matrices on $\mathcal{H}$). Using the two-design identities of the CUE, we find (*51*).

$$\Phi(O) = \frac{1}{3}\left(\mathrm{Tr}[O] - \frac{1}{2}\mathrm{Tr}[\mathbb{S}O]\right)\mathbb{1}_2 + \frac{1}{3}\left(\mathrm{Tr}[\mathbb{S}O] - \frac{1}{2}\mathrm{Tr}[O]\right)\mathbb{S}$$

where $\mathbb{S} = \sum_{s,s'} |s,s'\rangle\langle s',s|$ denotes the swap operator. We also define the closely related isotropic twirling channel (*52*)

$$\Psi(O) \equiv \overline{U^\dagger \otimes (U^*)^\dagger O U \otimes U^*} = [\Phi(O^{T_2})]^{T_2} \tag{10}$$

Here, $(\cdot)^{T_2}$ denotes the partial transpose with respect to the second spin. For the following proofs, we will use an operator $\widetilde{O} \equiv 2\sum_{s,s'} (-2)^{-D[s,s']} |s,s'\rangle\langle s,s'|$, which is diagonal in the computational basis, and fullfills (*51*)

$$\Phi(\widetilde{O}) = \mathbb{S}, \tag{11}$$

$$\Psi(\widetilde{O}) = \mathbb{S}^{T_2} = \sum_{s,s'} |s,s\rangle\langle s',s'| \equiv \mathbb{T} \tag{12}$$

In the following, we show how to use the identities (Eqs. 11 and 12) to prove Eqs. 3 to 6 relating randomized measurements and MBTIs.

Partial reflection invariant from randomized measurements

The MBTI $Z_{\mathcal{R}}$ is inferred from statistical correlations of randomized measurements, performed on a quantum state ρ_I, which are implemented by applying spatially correlated local random unitaries of the form $U_{\mathcal{R}} = \bigotimes_{i=1}^{2n} U_i$, with $U_i = U_{2n-i+1}$ for $i = 1, \ldots, n$. To prove Eq. 3, we first note that its right-hand side can be rewritten as an expectation value of an operator O_R

$$\begin{aligned}\mathcal{E}_{\mathcal{R}} &\equiv 2^n \sum_{s_I} (-2)^{-\frac{1}{2}D[s_I, \mathcal{R}_I(s_I)]} \overline{P_{U_{\mathcal{R}}}(s_I)} \\ &= \mathrm{Tr}\left[\overline{U_{\mathcal{R}}^\dagger O_{\mathcal{R}} U_{\mathcal{R}}} \rho_I\right] \\ &= \mathrm{Tr}\left[\bigotimes_{i=1}^{n} \overline{\left(U_i^\dagger \otimes U_i^\dagger\right) O_{\mathcal{R},i} \left(U_i \otimes U_i\right)} \rho_I\right]\end{aligned}$$

with $O_{\mathcal{R}} = \bigotimes_{i=1}^{n} O_{\mathcal{R},i}$, which is a tensor product of operators

$$O_{\mathcal{R},i} = 2\sum_{s_{I[i]}} (-2)^{-\frac{1}{2}D[s_{I[i]}, \mathcal{R}_I(s_{I[i]})]} |s_{I[i]}\rangle\langle s_{I[i]}| \tag{13}$$

acting on pairs of spins $I[i] = (i, 2n - i + 1)$. We also used the independence of the unitaries U_i and $U_{i'}$ (for $i \neq i'$ with $i, i' = 1, \ldots, n$)

applied to different pairs of spins $I[i]$ and $I[i']$, respectively. Using Eq. 11 with the identification $\mathcal{R}_{I[i]} \rightarrow \mathbb{S}$, and $O_{\mathcal{R},i} \rightarrow \widetilde{O}$, we find

$$\overline{\left(U_i^\dagger \otimes U_i^\dagger\right) O_{\mathcal{R},i} \left(U_i \otimes U_i\right)} = \mathcal{R}_{I[i]}$$

and therefore obtain

$$\mathcal{E}_{\mathcal{R}} = \mathrm{Tr}\left[\bigotimes_{i=1}^{n} \mathcal{R}_{I[i]}\, \rho_I\right] = \mathcal{Z}_{\mathcal{R}}$$

Partial time-reversal invariant from randomized measurements

The MBTI $Z_{\mathcal{T}}$ is inferred from the statistical correlations of correlated randomized measurements on two (sequential) experiments, both preparing a quantum state ρ_I. These are implemented by applying to the sites in an interval $I = I_1 \cup I_2$ local random unitaries $U_{\mathcal{T}}^{(1)} = U_{I_1} u_{\mathcal{T}} \otimes U_{I_2}$ (experiment 1) and $U_{\mathcal{T}}^{(2)} = U_{I_1}^* \otimes U_{I_2}$ (experiment 2) with $U_{I_{1,2}} = \otimes_{i \in I_{1,2}} U_i$ and $u_{\mathcal{T}} = \otimes_{i \in I_1} \sigma_i^y$, respectively. To prove Eq. 6, we rewrite its right-hand side as

$$\begin{aligned}
\mathcal{E}_{\mathcal{T}} &\equiv 2^{2n} \sum_{s_I, s_I'} (-2)^{-D[s_I, s_I']}\, \overline{P_{U_{\mathcal{T}}^{(1)}}(s_I)\, P_{U_{\mathcal{T}}^{(2)}}(s_I')} \\
&= \mathrm{Tr}\left[\overline{\left(U_{\mathcal{T}}^{(1)}\right)^\dagger \otimes \left(U_{\mathcal{T}}^{(2)}\right)^\dagger O_{\mathcal{T}} U_{\mathcal{T}}^{(1)} \otimes U_{\mathcal{T}}^{(2)}} \left(\rho_I \otimes \rho_I\right)\right] \\
&= \mathrm{Tr}\left[\bigotimes_{i \in I_1} \overline{U_i^\dagger \otimes \left(U_i^*\right)^\dagger O_{\mathcal{T},i} U_i \otimes U_i^*} \right. \\
&\quad \left. \bigotimes_{i \in I_2} \overline{U_i^\dagger \otimes U_i^\dagger O_{\mathcal{T},i} U_i \otimes U_i} \left(\tilde{\rho}_I \otimes \rho_I\right)\right]
\end{aligned} \tag{14}$$

Here, we have defined $\tilde{\rho}_I \equiv \left(u_{\mathcal{T}} \otimes 1_{I_2}\right) \rho_I \left(u_{\mathcal{T}}^\dagger \otimes 1_{I_2}\right)$ and used the (spatial) tensor product structure of the operator $O_{\mathcal{T}} = \otimes_{i \in I} O_{\mathcal{T},i}$ with

$$O_{\mathcal{T},i} = 2 \sum_{s_i, s_i'} (-2)^{-D[s_i, s_i']} |s_i\rangle\langle s_i| \otimes |s_i'\rangle\langle s_i'| \tag{15}$$

Using Eqs. 11 and 12 with the identification $\mathbb{S}_i \rightarrow \mathbb{S}$, $\mathbb{T}_i \rightarrow \mathbb{T}$, and $O_{\mathcal{T},i} \rightarrow \widetilde{O}$, we thus directly obtain

$$\begin{aligned}
\mathcal{E}_{\mathcal{T}} &= \mathrm{Tr}\left[\bigotimes_{i \in I_1} \mathbb{T}_i \bigotimes_{i \in I_2} \mathbb{S}_i \left(\tilde{\rho}_I \otimes \rho_I\right)\right] \\
&= \mathrm{Tr}\left[\left(\tilde{\rho}_I\right)^{T_{I_1}} \rho_I\right] = \mathcal{Z}_{\mathcal{T}}
\end{aligned} \tag{16}$$

Details on the DMRG and TEBD simulations

DMRG and TEBD simulations for the ground states and time-dependent states, respectively, were realized using the ITensor Library (http://itensor.org) in the framework of matrix product states. To get a ground state, the model was numerically solved with open-boundary conditions, with an additional small pinning field acting on the first site $\delta_p \sigma_1^z$, with $\delta_p = 0.05J$, to select one of the two degenerate ground states present in the topological phase for open boundary conditions (*53*). Note that in experiment with large system size N, the system would always choose one of the degenerate ground states because a cat state (i.e., the superposition of the two degenerate ground states) is always fragile to perturbations (as simulated by the small pinning field). We used a maximum bond dimension of $D = 512$. The quasi-exact MBTIs were extracted from direct contractions of the matrix product states representing the ground states (as shown by the solid lines in Figs. 1, 2, and 4). The estimations for randomized measurements were obtained using a sampling algorithm of the occupation probabilities P_U(s) for matrix product states (*54*).

The simulations for the time-dependent state for the adiabatic state preparation (as in Fig. 3) were realized via the TEBD algorithm with a time step $Jdt = 0.001$ and a maximum bond dimension $D = 512$.

SUPPLEMENTARY MATERIALS

Supplementary material for this article is available at http://advances.sciencemag.org/cgi/content/full/6/15/eaaz3666/DC1

REFERENCES AND NOTES

1. I. M. Georgescu, S. Ashhab, F. Nori, Quantum simulation. *Rev. Mod. Phys.* **86**, 153–185 (2014).
2. N. Goldman, J. C. Budich, P. Zoller, Topological quantum matter with ultracold gases in optical lattices. *Nat. Phys.* **12**, 639–645 (2016).
3. H. Weimer, M. Müller, I. Lesanovsky, P. Zoller, H. P. Büchler, A Rydberg quantum simulator. *Nat. Phys.* **6**, 382–388 (2010).
4. R. Blatt, C. F. Roos, Quantum simulations with trapped ions. *Nat. Phys.* **8**, 277–284 (2012).
5. A. A. Houck, H. E. Türeci, J. Koch, On-chip quantum simulation with superconducting circuits. *Nat. Phys.* **8**, 292–299 (2012).
6. D. C. Tsui, H. L. Stormer, A. C. Gossard, Two-dimensional magnetotransport in the extreme quantum limit. *Phys. Rev. Lett.* **48**, 1559–1562 (1982).
7. R. B. Laughlin, Anomalous quantum Hall effect: An incompressible quantum fluid with fractionally charged excitations. *Phys. Rev. Lett.* **50**, 1395–1398 (1983).
8. C. Nayak, S. H. Simon, A. Stern, M. Freedman, S. Das Sarma, Non-abelian anyons and topological quantum computation. *Rev. Mod. Phys.* **80**, 1083–1159 (2008).
9. V. Ginzburg, L. Landau, On the theory of superconductivity. *Zh. Eksp. Teor. Fiz.* **20**, 1064–1082 (1950).
10. M. Atala, M. Aidelsburger, J. T. Barreiro, D. Abanin, T. Kitagawa, E. Demler, I. Bloch, Direct measurement of the Zak phase in topological Bloch bands. *Nat. Phys.* **9**, 795–800 (2013).
11. M. Aidelsburger, M. Lohse, C. Schweizer, M. Atala, J. T. Barreiro, S. Nascimbène, N. R. Cooper, I. Bloch, N. Goldman, Measuring the Chern number of Hofstadter bands with ultracold bosonic atoms. *Nat. Phys.* **11**, 162–166 (2015).
12. M. Lohse, C. Schweizer, O. Zilberberg, M. Aidelsburger, I. Bloch, A Thouless quantum pump with ultracold bosonic atoms in an optical superlattice. *Nat. Phys.* **12**, 350–354 (2016).
13. S. Nakajima, T. Tomita, S. Taie, T. Ichinose, H. Ozawa, L. Wang, M. Troyer, Y. Takahashi, Topological Thouless pumping of ultracold fermions. *Nat. Phys.* **12**, 296–300 (2016).
14. W. Hu, J. C. Pillay, K. Wu, M. Pasek, P. P. Shum, Y. D. Chong, Measurement of a topological edge invariant in a microwave network. *Phys. Rev. X* **5**, 011012 (2015).
15. S. Mittal, S. Ganeshan, J. Fan, A. Vaezi, M. Hafezi, Measurement of topological invariants in a 2D photonic system. *Nat. Photonics* **10**, 180–183 (2016).
16. J. Haegeman, D. Pérez-García, I. Cirac, N. Schuch, Order parameter for symmetry-protected phases in one dimension. *Phys. Rev. Lett.* **109**, 050402 (2012).
17. F. Pollmann, A. M. Turner, Detection of symmetry-protected topological phases in one dimension. *Phys. Rev. B* **86**, 125441 (2012).
18. Z.-C. Gu, X.-G. Wen, Tensor-entanglement-filtering renormalization approach and symmetry-protected topological order. *Phys. Rev. B* **80**, 155131 (2009).
19. X. Chen, Z.-C. Gu, Z.-X. Liu, X.-G. Wen, Symmetry-protected topological orders in interacting bosonic systems. *Science* **338**, 1604–1606 (2012).
20. M. den Nijs, K. Rommelse, Preroughening transitions in crystal surfaces and valence-bond phases in quantum spin chains. *Phys. Rev. B* **40**, 4709–4734 (1989).
21. M. Endres, M. Cheneau, T. Fukuhara, C. Weitenberg, P. Schauß, C. Gross, L. Mazza, M. C. Bañuls, L. Pollet, I. Bloch, S. Kuhr, Observation of correlated particle-hole pairs and string order in low-dimensional Mott insulators. *Science* **334**, 200–203 (2011).
22. S. de Léséleuc, V. Lienhard, P. Scholl, D. Barredo, S. Weber, N. Lang, H. P. Büchler, T. Lahaye, A. Browaeys, Observation of a symmetry-protected topological phase of interacting bosons with Rydberg atoms. *Science* **365**, 775 (2019).
23. F. Pollmann, A. M. Turner, E. Berg, M. Oshikawa, Entanglement spectrum of a topological phase in one dimension. *Phys. Rev. B* **81**, 064439 (2010).
24. H. Shapourian, K. Shiozaki, S. Ryu, Many-body topological invariants for fermionic symmetry-protected topological phases. *Phys. Rev. Lett.* **118**, 216402 (2017).

25. K. Shiozaki, S. Ryu, Matrix product states and equivariant topological field theories for bosonic symmetry-protected topological phases in (1+1) dimensions. *J. High Energy Phys.* **2017**, 100 (2017).
26. K. Shiozaki, H. Shapourian, K. Gomi, S. Ryu, Many-body topological invariants for fermionic short-range entangled topological phases protected by antiunitary symmetries. *Phys. Rev. B* **98**, 035151 (2018).
27. R. Verresen, R. Thorngren, N. G. Jones, F. Pollmann, Gapless topological phases and symmetry-enriched quantum criticality. arXiv:1905.06969 [cond-mat.str-el] (16 May 2019).
28. C.-Y. Huang, X. Chen, F. Pollmann, Detection of symmetry-enriched topological phases. *Phys. Rev. B* **90**, 045142 (2014).
29. M. Barkeshli, P. Bonderson, M. Cheng, C.-M. Jian, K. Walker, Reflection and time reversal symmetry enriched topological phases of matter: Path integrals, non-orientable manifolds, and anomalies. *Commun. Math. Phys.* **374**, 1021–1124 (2020).
30. S. J. van Enk, C. W. J. Beenakker, Measuring Tr ρ^n on single copies of ρ using random measurements. *Phys. Rev. Lett.* **108**, 110503 (2012).
31. A. Elben, B. Vermersch, M. Dalmonte, J. I. Cirac, P. Zoller, Rényi entropies from random quenches in atomic Hubbard and spin models. *Phys. Rev. Lett.* **120**, 050406 (2018).
32. T. Brydges, A. Elben, P. Jurcevic, B. Vermersch, C. Maier, B. P. Lanyon, P. Zoller, R. Blatt, C. F. Roos, Probing Rényi entanglement entropy via randomized measurements. *Science* **364**, 260–263 (2019).
33. B. Vermersch, A. Elben, L. M. Sieberer, N. Y. Yao, P. Zoller, Probing scrambling using statistical correlations between randomized measurements. *Phys. Rev. X* **9**, 021061 (2019).
34. W. P. Su, J. R. Schrieffer, A. J. Heeger, Solitons in polyacetylene. *Phys. Rev. Lett.* **42**, 1698–1701 (1979).
35. R. M. Lynden-Bell, H. M. McConnell, Theory of paramagnetic excitons in solid free radicals. *J. Chem. Phys.* **37**, 794–798 (1962).
36. K. Hida, Crossover between the Haldane-gap phase and the dimer phase in the spin-1/2 alternating Heisenberg chain. *Phys. Rev. B* **45**, 2207–2212 (1992).
37. F. Grusdt, M. Höning, M. Fleischhauer, Topological edge states in the one-dimensional superlattice Bose-Hubbard model. *Phys. Rev. Lett.* **110**, 260405 (2013).
38. D. González-Cuadra, P. R. Grzybowski, A. Dauphin, M. Lewenstein, Strongly correlated bosons on a dynamical lattice. *Phys. Rev. Lett.* **121**, 090402 (2018).
39. D. González-Cuadra, A. Dauphin, P. R. Grzybowski, P. Wójcik, M. Lewenstein, A. Bermudez, Symmetry-breaking topological insulators in the $\mathbb{Z}_2$ Bose-Hubbard model. *Phys. Rev. B* **99**, 045139 (2019).
40. F. D. M. Haldane, Nonlinear field theory of large-spin heisenberg antiferromagnets: Semiclassically quantized solitons of the one-dimensional easy-axis Néel state. *Phys. Rev. Lett.* **50**, 1153–1156 (1983).
41. F. Pollmann, E. Berg, A. M. Turner, M. Oshikawa, Symmetry protection of topological phases in one-dimensional quantum spin systems. *Phys. Rev. B* **85**, 075125 (2012).
42. A. Elben, B. Vermersch, R. van Bijnen, C. Kokail, T. Brydges, C. Maier, M. Joshi, R. Blatt, C. F. Roos, P. Zoller, Cross-platform verification of intermediate scale quantum devices. *Phys. Rev. Lett.* **124**, 010504 (2020).
43. M. McGinley, N. R. Cooper, Topology of one-dimensional quantum systems out of equilibrium. *Phys. Rev. Lett.* **121**, 090401 (2018).
44. M. P. Zaletel, Detecting two-dimensional symmetry-protected topological order in a ground-state wave function. *Phys. Rev. B* **90**, 235113 (2014).
45. A. M. Essin, M. Hermele, Classifying fractionalization: Symmetry classification of gapped $\mathbb{Z}_2$ spin liquids in two dimensions. *Phys. Rev. B* **87**, 104406 (2013).
46. J. Garre-Rubio, S. Iblisdir, Local order parameters for symmetry fractionalization. *New J. Phys.* **21**, 113016 (2019).
47. F. Grusdt, N. Y. Yao, D. Abanin, M. Fleischhauer, E. Demler, Interferometric measurements of many-body topological invariants using mobile impurities. *Nat. Commun.* **7**, 11994 (2016).
48. C. Repellin, N. Goldman, Detecting fractional Chern insulators through circular dichroism. *Phys. Rev. Lett.* **122**, 166801 (2019).
49. X.-G. Wen, Topological orders in rigid states. *Int. J. Mod. Phys. B* **4**, 239–271 (1990).
50. G. Zhu, M. Hafezi, M. Barkeshli, Quantum origami: Transversal gates for quantum computation and measurement of topological order. arXiv:1711.05752 [quant-ph] (15 November 2017).
51. A. Elben, B. Vermersch, C. F. Roos, P. Zoller, Statistical correlations between locally randomized measurements: A toolbox for probing entanglement in many-body quantum states. *Phys. Rev. A* **99**, 052323 (2019).
52. J. Watrous, *The Theory of Quantum Information* (Cambridge Univ. Press, 2018).
53. G. De Chiara, L. Lepori, M. Lewenstein, A. Sanpera, Entanglement spectrum, critical exponents, and order parameters in quantum spin chains. *Phys. Rev. Lett.* **109**, 237208 (2012).
54. Z.-Y. Han, J. Wang, H. Fan, L. Wang, P. Zhang, Unsupervised generative modeling using matrix product states. *Phys. Rev. X* **8**, 031012 (2018).

Acknowledgments: We thank the PASQuanS partners and Z. P. Cian, I. Cirac, M. Hermele, M. Knap, and Z.-X. Liu for discussions. The tensor-network simulations (DMRG and TEBD) were realized using the ITensor Library (http://itensor.org). **Funding:** Research in Innsbruck is supported by the European Research Council (ERC) under the European Union's Horizon 2020 research and innovation programme (Grant Agreement No. 741541), and from the European Union's Horizon 2020 research and innovation programme under Grant Agreement No. 817482 (Pasquans) and No. 731473 (FWF QuantERA via QTFLAG I03769). Furthermore, this work was supported by the Simons Collaboration on UltraQuantum Matter, which is a grant from the Simons Foundation (651440, P.Z.). Research in Maryland was supported by ARO-MURI and NSF-PFC at the JQI. F.P. acknowledges funding from the Deutsche Forschungsgemeinschaft (DFG, German Research Foundation) under Germany's Excellence Strategy—EXC-2111-390814868, DFG TRR80 (project number 107745057), DFG Research Unit FOR 1807 through grant no. PO 1370/2-1, the ERC under the European Unions Horizon 2020 research, and innovation program grant agreement no. 771537. **Author contributions:** A.E., G.Z., P.Z., and B.V. proposed the research project. A.E. and B.V. derived the randomized measurement protocols to access MBTIs. A.E. and J.Y. performed the numerical simulations. A.E., J.Y., G.Z., M.H., F.P., P.Z., and B.V. contributed to the interpretations of the numerical simulations and wrote the manuscript. **Competing interests:** The authors declare that they have no competing interests. **Data and materials availability:** All data needed to evaluate the conclusions in the paper are present in the paper and/or the Supplementary Materials. Additional data related to this paper may be requested from the authors.

Submitted 4 September 2019
Accepted 9 January 2020
Published 10 April 2020
10.1126/sciadv.aaz3666

Citation: A. Elben, J. Yu, G. Zhu, M. Hafezi, F. Pollmann, P. Zoller, B. Vermersch, Many-body topological invariants from randomized measurements in synthetic quantum matter. *Sci. Adv.* **6**, eaaz3666 (2020).

Science Advances

Many-body topological invariants from randomized measurements in synthetic quantum matter

Andreas Elben, Jinlong Yu, Guanyu Zhu, Mohammad Hafezi, Frank Pollmann, Peter Zoller and Benoît Vermersch

Sci Adv **6** (15), eaaz3666.
DOI: 10.1126/sciadv.aaz3666

Science Advances (ISSN 2375-2548) is published by the American Association for the Advancement of Science, 1200 New York Avenue NW, Washington, DC 20005. The title *Science Advances* is a registered trademark of AAAS.